

# Numerical study on three-dimensional flow effect of self-ignition induced by high pressure hydrogen jet in a rectangular tube

Akinori Yokoyama\*, Makoto Asahara\*<sup>†</sup>, Nobuyuki Tsuboi\*\*\*, and A. Koichi Hayashi\*

\*Aoyama Gakuin University, 5-10-1 Fuchinobe, Chuo-ku, Sagami-hara, Kanagawa 252-0206, JAPAN

Phone : +81-42-759-6509

<sup>†</sup>Corresponding author : e-mail : asahara@me.aoyama.ac.jp

\*\*Kyushu Institute of Technology, 1-1 Sensui-cho, Tobata-ku, Kitakyushu, Fukuoka 804-8550, JAPAN

Received : November 13, 2014 Accepted : October 2, 2015

## Abstract

Self-ignition in high-pressure hydrogen jets may take place when transverse shock waves are generated from diaphragm transformation. In this study, a numerical analysis was performed to find out the mechanism of self-ignition in a high-pressure hydrogen jet in a tube. High-pressure hydrogen and air at the atmospheric pressure were mixed to yield vortices in the boundary layer and at the contact surface. The high temperature and high-pressure atmosphere in the mixing region, and the generation of a precursor shock wave following the flow of hydrogen under such high-pressure conditions, caused self-ignition. A numerical simulation showed that the ignition happens within the vortices in the tube.

**Keywords** : self-ignition, hydrogen, shock wave, contact surface, transverse wave

## 1. Introduction

In order to encourage the use of hydrogen energy, it is necessary to establish safe storage and shipping technologies for hydrogen. Hydrogen is normally stored in high-pressure tanks to increase storage efficiency. When the pressure in hydrogen tanks becomes too high, hydrogen is released through a tube to decrease the pressure. According to some of the reported incidents, hydrogen can ignite during this process without the presence of any ignition source. This is called "hydrogen self-ignition." For hydrogen to be more commonly used, the cause of self-ignition must be investigated.

Various studies on hydrogen self-ignition that focused on observing flames at the exit of the tube have been performed<sup>1)-12)</sup>. It is very important studies that were investigated the conditions of observing flames at the exit of the tube. When high-pressure hydrogen is released to ambient air, self-ignition occurs because of a temperature rise caused by a shock wave creating a temperature gradient that reaches the self-ignition temperature. Wolanski and Wojcicki<sup>1)</sup> experimentally observed self-ignition for the first time in 1973. Recently, Mogi et al.<sup>6)</sup>

found that self-ignition occurred more readily when the length of the tube, used for releasing the pressure inside a storage tank, was longer and initial pressure was higher. However, Kitabayashi et al.<sup>8)</sup> reported that self-ignition no longer occurred at the same pressure, whereas Mogi et al.<sup>6)</sup> observed self-ignition when using a tube length of 1.2m. This tube length was longer than that used by Mogi et al.<sup>6)</sup>, however, the difference in the observations was likely due to the different experimental conditions, which caused friction loss and heat transfer to walls. The experiments by Kitabayashi et al.<sup>8)</sup> proved that self-ignition may not occur even if long tubes are used and concluded that the phenomenon cannot be studied by only observing a flame at the tube exit. Dryer et al.<sup>13)</sup> also analyzed the phenomenon of ignition inside the pressure-release tube. In their experiment, Dryer et al.<sup>13)</sup> released hydrogen into the air and found that the self-ignition occurred inside the inner tube. Since the pressure difference between high-pressure hydrogen and ambient pressure air is large, a diaphragm transformation occurs before bursting. The self-ignition was likely caused by the local rise in the temperature at a reflection of a transverse

shock wave, generated by the rupture of the transformed diaphragm, on wall. However, Dryer *et al.*<sup>13)</sup> did not observe such details. Then, the studies focused on phenomena at inner tube are performed<sup>14)–22)</sup>. Studies cited here is also very important to elucidate the self-ignition in the tube. Kim *et al.*<sup>19)</sup> performed the experiments using a rectangular tube with a visualization window and reported that self-ignition occurred at the boundary layer. A mixing zone was developed along the boundary layers and the ignition area spread into the mixing zone. However, Kim *et al.*<sup>19)</sup> did not show the mixing process near the tube wall. Asahara *et al.*<sup>20)</sup> simulated the experiments by Kim *et al.*<sup>19)</sup> in a two-dimensional space and clarified the mixing gases were formed by hydrodynamic instability near the tube wall.

Based on the research so far, the mechanism of self-ignition cannot be discussed quantitatively because self-ignition is difficult to reproduce experimentally and the observations are unclear. It is assumed that the self-ignition limit and the effect of tube shape and size are difficult to visualize in experiments. In this study, self-ignition inside a three-dimensional rectangular tube is the basis for developing a numerical model to compare with the experimental results from Kim *et al.*<sup>19)</sup> The numerical model also shows the process of ignition near the boundary layer that Kim *et al.*<sup>19)</sup> were unable to show in detail.

## 2. Numerical method

The governing equations for the numerical simulation are the three-dimensional compressible Navier-Stokes equations with the equation for conservation of mass of each chemical species (Equations 1 and 2).

$$\frac{\partial \mathbf{Q}}{\partial t} + \frac{\partial \mathbf{E}}{\partial x} + \frac{\partial \mathbf{F}}{\partial y} + \frac{\partial \mathbf{G}}{\partial z} = \frac{\partial \mathbf{E}_d}{\partial x} + \frac{\partial \mathbf{F}_d}{\partial y} + \frac{\partial \mathbf{G}_d}{\partial z} + \mathbf{S} \quad (1)$$

$$\mathbf{Q} = \begin{pmatrix} \rho \\ \rho u \\ \rho v \\ \rho w \\ e \\ \rho_i \end{pmatrix} \quad \mathbf{E} = \begin{pmatrix} \rho u \\ \rho u^2 + p \\ \rho uv \\ \rho uw \\ (e+p)u \\ \rho_i u \end{pmatrix} \quad \mathbf{F} = \begin{pmatrix} \rho v \\ \rho v u \\ \rho v^2 + p \\ \rho vw \\ (e+p)v \\ \rho_i v \end{pmatrix} \quad \mathbf{G} = \begin{pmatrix} \rho w \\ \rho w u \\ \rho w v \\ \rho w^2 + p \\ (e+p)w \\ \rho_i w \end{pmatrix}$$

$$\mathbf{E}_d = \begin{pmatrix} 0 \\ \tau_{xx} \\ \tau_{xy} \\ \tau_{xz} \\ \tau_{xx}u + \tau_{xy}v + \tau_{xz}w - q_x \\ \rho D_i \frac{\partial Y_i}{\partial x} \end{pmatrix} \quad \mathbf{F}_d = \begin{pmatrix} 0 \\ \tau_{yx} \\ \tau_{yy} \\ \tau_{yz} \\ \tau_{yx}u + \tau_{yy}v + \tau_{yz}w - q_y \\ \rho D_i \frac{\partial Y_i}{\partial y} \end{pmatrix}$$

$$\mathbf{G}_d = \begin{pmatrix} 0 \\ \tau_{zx} \\ \tau_{zy} \\ \tau_{zz} \\ \tau_{zx}u + \tau_{zy}v + \tau_{zz}w - q_z \\ \rho D_i \frac{\partial Y_i}{\partial z} \end{pmatrix} \quad \mathbf{W} = \begin{pmatrix} 0 \\ 0 \\ 0 \\ 0 \\ 0 \\ \dot{\omega}_i \end{pmatrix} \quad (2)$$

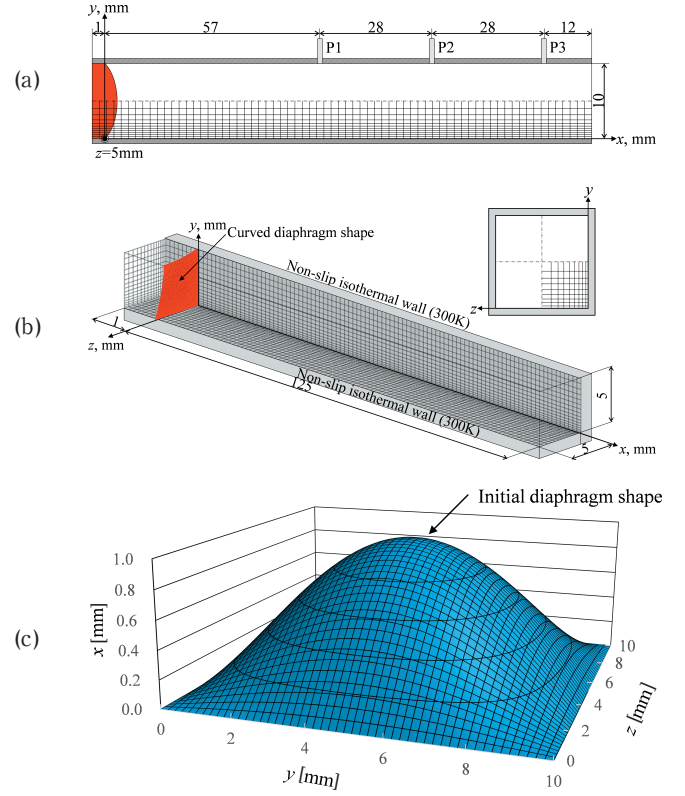


**Figure 1** Numerical models, (a): two-dimensional schematic figure of grid system with sensor positions, (b): schematic figure of grid system, (c): initial shape of the diaphragm.

where  $\rho$  is the density,  $u$  is the velocity in the  $x$ -direction,  $v$  is the velocity in the  $y$ -direction,  $w$  is the velocity in the  $z$ -direction,  $e$  is total energy,  $\rho_i$  is the density of each chemical species,  $p$  is pressure,  $\tau$  is shear stress,  $q$  is heat flux,  $D$  is effective diffusion coefficient, and  $Y$  is mass fraction.

These equations were integrated using the Strang-type time-split method<sup>23)</sup> for the unsteady term, a Harten-Yee's second-order explicit upwind total variation diminishing (TVD) scheme<sup>24)</sup> for the convective terms, a second-order central difference scheme for the diffusion terms, and a point-implicit method for the production terms. A chemical kinetics model developed by Hong *et al.*<sup>25)</sup> was used to calculate combustion, which has 9 species,  $\text{H}_2$ ,  $\text{O}_2$ ,  $\text{O}$ ,  $\text{H}$ ,  $\text{OH}$ ,  $\text{HO}_2$ ,  $\text{H}_2\text{O}_2$ ,  $\text{H}_2\text{O}$ , and  $\text{N}_2$ , and 20 elementary reactions. The equation based on the Lennard-Jones model<sup>26)</sup> was applied to calculate the transport coefficients, and the Wilke's law<sup>27)</sup> was used to calculate the coefficient of molecular viscosity.

Figure 1 shows a schematic grid system of the rectangular shock tube. The tube is the size originally used in the experiments by Kim *et al.*<sup>19)</sup> The length in the  $x$ -direction is 125 mm long because self-ignition occurs inside of the tube at the distance of 100 mm from the ignition point in the experiments by Kim *et al.* This distance is also supported by our past two-dimensional numerical analysis<sup>20)</sup>. The sizes of the  $y$ - and  $z$ -directions are the same as that of the experimental tube. It is assumed that the vertical and horizontal symmetries are set for the calculation with respect to the tube cross section. The wall boundary conditions are non-slip and

**Table 1** Initial conditions of simulation in the present study.

	High-pressure area	Ambient pressure area
$P$ [MPa]	9.0	0.1
$T$ [K]	300	300
Gas	H <sub>2</sub>	Air

isothermal. The wall temperature is 300 K. The grid size in the  $x$ -direction is 50  $\mu\text{m}$ , and in the  $y$ - and  $z$ -directions are from 10  $\mu\text{m}$  to 57  $\mu\text{m}$ , which are set finer near the walls. The number of grids for the  $x$ -,  $y$ -,  $z$ -directions is 2521, 151, and 151, respectively. The initial conditions for the calculation are shown in Table 1. The hydrogen pressure is 9.0 MPa and hydrogen temperature is 300 K in the high-pressure area. The air pressure is 0.1 MPa and its temperature is 300 K in the ambient pressure area. The shape of the diaphragm is obtained by solving the bending problem of an elastic body with a distributed load using a fourth-order function. In this work, the reaction flame configuration is investigated when high-pressure hydrogen and air at the ambient pressure are mixed at a temperature of over 2400 K.

### 3. Results and discussion

#### 3.1 Validation of calculation

The validation of the numerical results was performed using a time history of pressure in the tube. Figure 2 shows the time history of two pressure sensors (P1 and P3), where the horizontal axis indicates time and the vertical axis indicates pressure. The sensors are set at 57 mm (P1) and 113 mm (P3) from the wall in the  $x$ -direction. The time history of the pressure sensor at 85 mm (P2) in the experiments by Kim et al.<sup>19)</sup> had a lot of noise. Therefore, we cannot compare our numerical data with Kim et al.'s<sup>19)</sup> experimental data. Since Kim et al.<sup>19)</sup> used the pressure sensors with the diameter of 6.3 mm (Kulite, ETM HT 375-5000G), the numerical pressure is obtained using the average value of the similar size, as their data near the pressure sensor on the wall. The initial rise in the pressure and the process of its subsequent increase are accurately simulated for a comparison with the experiments by Kim et al.<sup>19)</sup>, as shown in Figure 2. The figure also provides the accuracy of each pressure sensor. The propagating velocity of the leading shock wave was

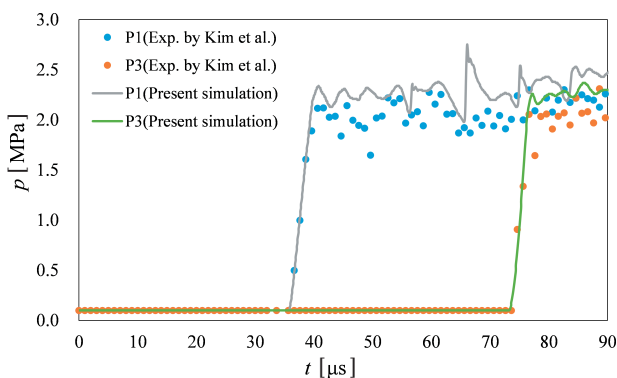


**Figure 2** Comparison of the time history of sensor pressures, P1 ( $x = 57$  mm) and P3 ( $x = 113$  mm), between the present simulation and the experiments by Kim et al.<sup>19)</sup>

also obtained from the numerical simulation, where the initial rise in the pressure sensors indicates the arrival of the leading shock wave. After the initial rise of pressure, the pressure profiles in the simulation fluctuated at approximately 2.2 MPa, whereas the pressure profiles in the experiment by Kim et al.<sup>19)</sup> vibrated at approximately 2.0 MPa. This is because the experimental diaphragm might not have been ruptured as homogeneously and instantaneously as that in the numerical results, and thus the high-pressure hydrogen may have propagated gradually through the experimental tube. The present calculation is valid, because the pressure rise-up time in the numerical results fits quantitatively with the experimental ones of Kim et al.<sup>19)</sup>, and the results of the subsequent pressure profile behavior fits qualitatively with the experimental values.

#### 3.2 Propagation process

Figure 3 shows the time history of the temperature contours at the distance  $z$  of 5.0 mm. The contact surface of hydrogen and air propagated behind the leading shock wave. The velocity of leading shock wave estimated from Figure 3 is  $1495 \text{ ms}^{-1}$ , it of contact surface is  $1107 \text{ ms}^{-1}$ . Theoretical leading shock velocity is  $1513 \text{ ms}^{-1}$  and it of contact surface is  $1195 \text{ ms}^{-1}$ . The difference of numerical velocity and theoretical velocity are 1.19 % and 7.36 % respectively. From Figure 3, self-ignition occurs at contact surface. Figure 4 shows the isosurfaces of vorticity at  $9.0 \times 10^5 \text{ s}^{-1}$ , and Figure 5 shows the isosurface of temperature at 2400 K which means the flame configuration. Self-ignition occurred near the wall behind

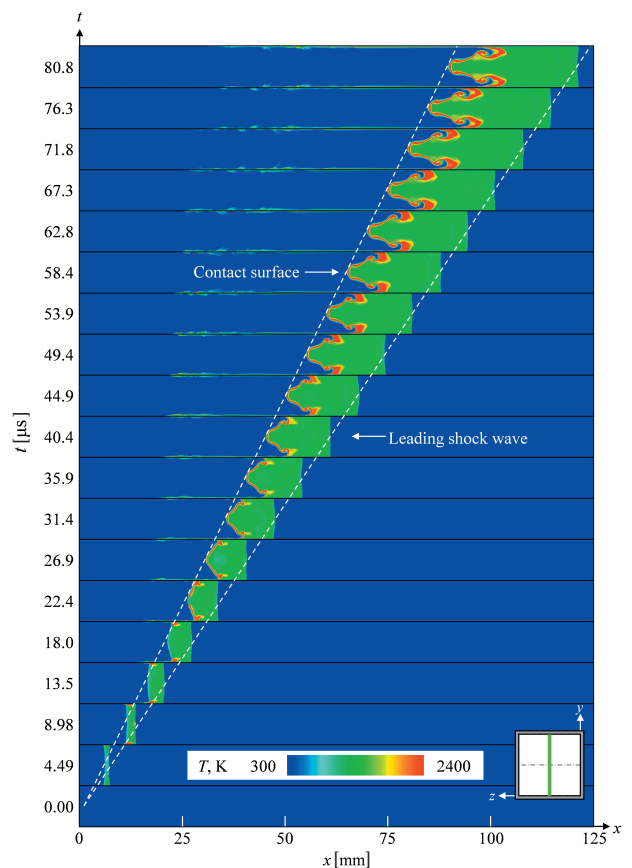


**Figure 3** Time history of the contours of temperature.

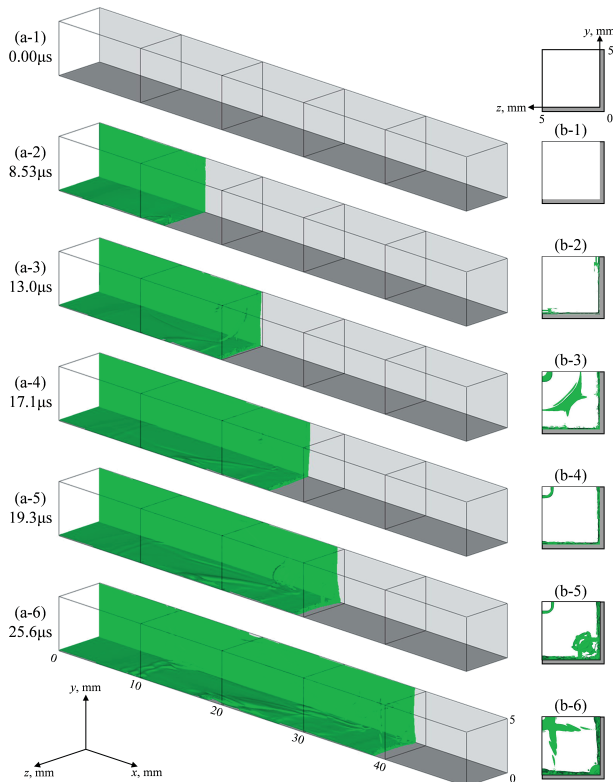


**Figure 4** Time history of the isosurfaces of vorticity at  $9.0 \times 10^5 \text{ s}^{-1}$ , (a): three-dimensional images (b): projections of  $x$ -direction.

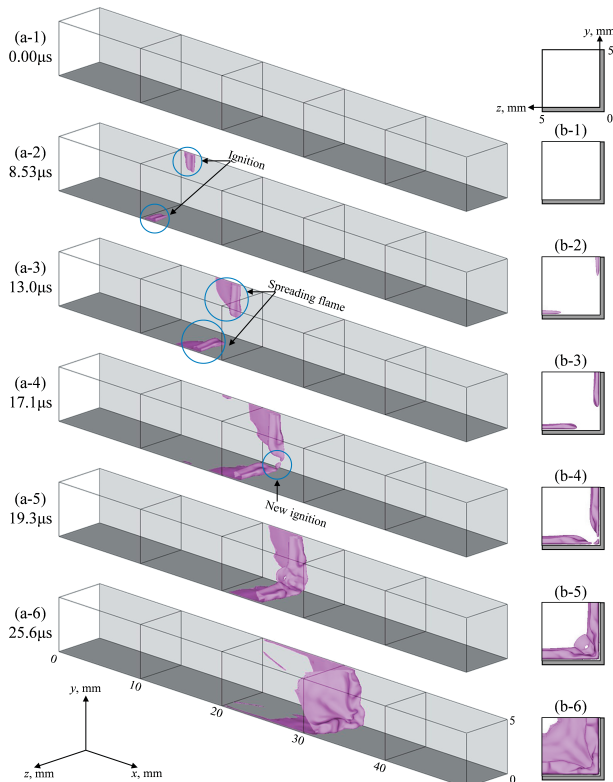


**Figure 5** Time history of the isosurfaces of temperature at 2400 K, (a): three-dimensional images (b): projections of  $x$ -direction.

the contact surface at the location of high vorticity at 8.53  $\mu\text{s}$ . Subsequently, the ignition area spread along the tube wall. Then another ignition occurred near the tube corner at 17.1  $\mu\text{s}$ . After this, the flame propagated out from the

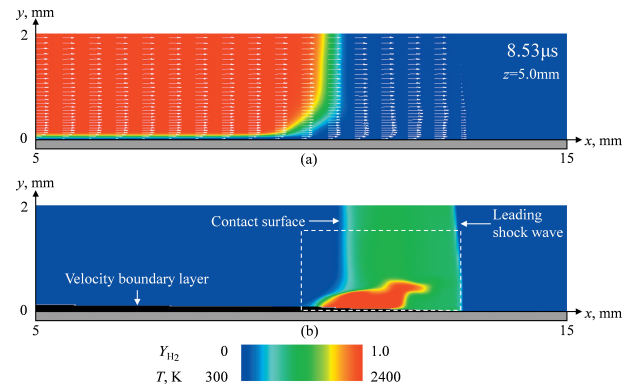


**Figure 6** Contours at the distance  $z$  of 5.0 mm at 8.53  $\mu\text{s}$ , (a):  $\text{H}_2$  mass fraction and velocity vector (b): temperature and velocity boundary layer.

tube corner to the center of the tube cross-section, and then to the whole contact surface at 25.7  $\mu\text{s}$ .

### 3.3 Self-ignition mechanism

Figure 6 shows the contours of (a)  $\text{H}_2$  mass fraction with velocity vectors and (b) temperature and velocity boundary layer at the distance  $z$  of 5.0 mm and at a time of 8.53  $\mu\text{s}$ . Here, the velocity boundary layer is defined by 99% velocity line of main flow. There is air near the tube wall near the velocity boundary layer. Figure 7 shows the zoomed in distribution of the density gradient (numerical Schlieren photos), the  $\text{H}_2$  mass fraction, temperature, and the  $\text{HO}_2$  mass fraction near the contact surface just before and at the time of self-ignition. There are locally high temperature areas due to the distributions of the density gradient and temperature. The transverse shock waves are reflected on the tube wall. The schematics in Figure 8 show the summary of the phenomena. In the flame,  $\text{HO}_2$  is yielded by the initiation reactions. This flame develops from high local temperatures due to the transverse shock wave. Then chemical reactions start, and self-ignition occurs at 8.53  $\mu\text{s}$  with some ignition delay.

### 3.4 The effect of the tube corner

Figure 9 shows the temperature isosurface and the density gradient contours (numerical Schlieren photos), temperature, and pressure at the distances  $x$  of 19.70, 20.85, and 22.00 mm and at the times of 15.3, 16.2, and 17.1  $\mu\text{s}$ . From this figure, a new self-ignition is recognized because a flame is formed independently from the first ignition. It is seen from the density gradient that the transverse shock wave propagates from the tube corner. This shows that new self-ignition occurs because of the transverse shock wave. The reason for the time difference between the self-ignition and the ignition described in Section 3.3 is due to the difference in times at which each transverse shock wave reaches the tube wall. After the transverse wave reaches to the wall, the flame propagates along the entire contact surface by the time of 25.6  $\mu\text{s}$ . Figure 10 shows a summary of the process of development of the flame, where (a) shows self-ignition at center of the wall, (b) shows new self-ignition at the corner of the tube, and (c) shows flame propagation.

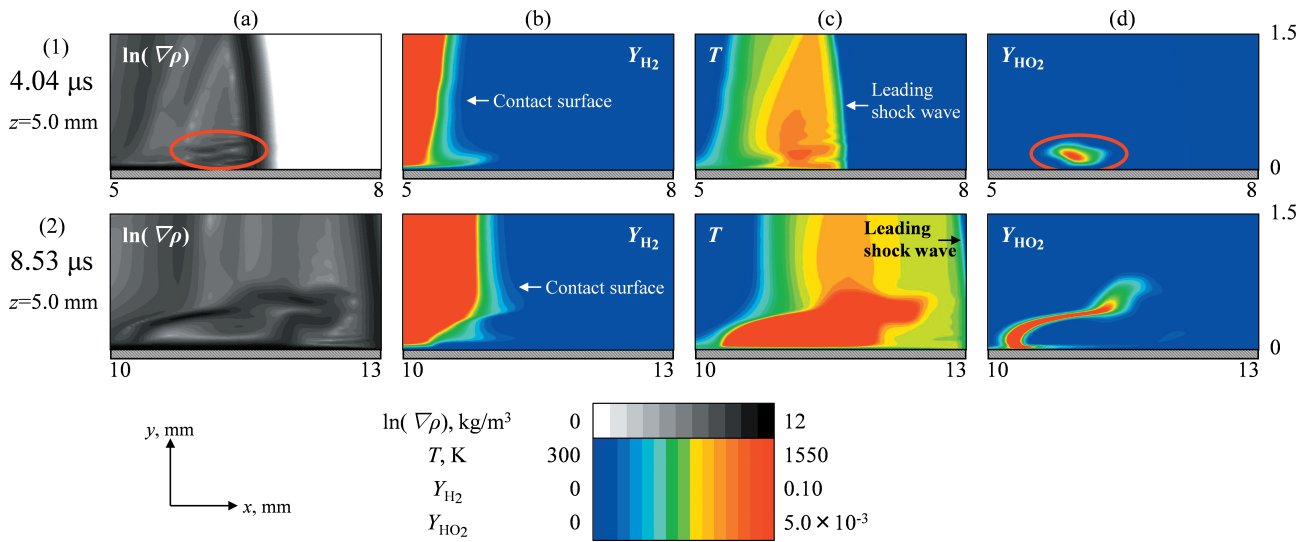


**Figure 7** Contours at the distance  $z$  of 5.0 mm at 4.04  $\mu$ s and 8.53  $\mu$ s, (a): density gradient (b): mass fraction of hydrogen (c): temperature (d): mass fraction of  $\text{HO}_2$ .

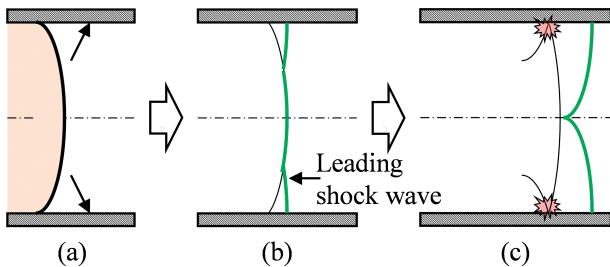


**Figure 8** Structure of a transverse shock wave, green line: leading shock wave, black line: transverse shock wave, (a): diaphragm shape (b): reflecting shock wave (c): rise the local temperature and pressure.

### 4. Conclusions

The three-dimensional numerical simulation of high-pressure hydrogen flow in the rectangular tube was performed by focusing on the self-ignition phenomena in the tube and the following findings were obtained:

- After the transverse shock wave reflects at the tube wall, the temperature increases, the chemical reactions are enhanced, and self-ignition starts.
- A new self-ignition occurs at the tube corner

### 5. Acknowledgment

We are grateful to Osaka University for the use of their super computer system.

### References

- 1) P. Wolanski and S. Wojcicki, Proceedings of the Combustion Institute, 14, 1217–1223 (1973).
- 2) V.V. Golub, D.I. Baklanov, T.V. Bazhenova, M.V. Bragin, S.V. Glovastov, M.F. Ivanov, and V.V. Volodin, Journal of Loss Prevention in the Process Industries, 20, Issues 4–6, 439–446 (2007).
- 3) V.V. Golub, D.I. Baklanov, S.V. Glovastov, M.F. Ivanov, I.N. Laskin, A.S. Saveliev, N.V. Semin, and V.V. Volodin, Journal of Loss Prevention in the Process Industries, 21, 185–198 (2008).
- 4) V.V. Golub, D.I. Baklanov, T.V. Bazhenova, S.V. Glovastov, M.F. Ivanov, I.N. Laskin, N.V. Semin, and V.V. Volodin,

- International Journal of Hydrogen Energy, 34, 5946–5953 (2009).
- 5) T. Mogi, D. Kim, H. Shiina, and S. Horiguchi, Journal of Loss Prevention in the Process Industries, 21, 199–204 (2008).
- 6) T. Mogi, Y. Wada, Y. Ogata, and A.K. Hayashi, International Journal of Hydrogen Energy, 34, 5810–5816 (2009).
- 7) B.P. Xu, J.X. Wen, and V.H.Y. Tam, International Journal of Hydrogen Energy, 36, 2637–2644 (2011).
- 8) N. Kitabayashi, Y. Wada, T. Mogi, T. Saburi, and A.K. Hayashi, International Journal of Hydrogen Energy, 38, 8100–8107 (2012).
- 9) S. Xiaobo and S. Jinhua, Physics Procedia, 33, 1833–1841 (2012).
- 10) M.V. Bragin, D.V. Makarov, and V.V. Molokov, International Journal of Hydrogen Energy, 38, 8039–8052 (2014).
- 11) W. Rudy, A. Dabkowski, and A. Teodorczyk, International Journal of Hydrogen Energy, 39, 20388–20395 (2014).
- 12) Q. Duan, H. Xiao, W. Gao, Q. Wang, X. Shen, L. Jiang, and J. Sun, International Journal of Hydrogen Energy, 40, 8281–8289 (2015).
- 13) F.L. Dryer, M. Chaos, Z. Zhao, J.N. Stein, J.Y. Alpert, and C.J. Homer, Combustion Science Technology, 179, 663–694 (2007).
- 14) B.P. Xu, L.I. Hima, J.X. Wen, S. Dembele, V.H.Y. Tam, and T. Donchev, Journal of Loss Prevention in the Process Industries, 21, 205–213 (2008).
- 15) B.P. Xu, J.X. Wen, S. Dembele, V.H.Y. Tam, and S.J. Hauksworth, Journal of Loss Prevention in the Process Industries, 22, 279–287 (2009).
- 16) B.P. Xu, L.I. Hima, J.X. Wen, and V.H.Y. Tam, International Journal of Hydrogen Energy, 34, 5945–5960 (2009).
- 17) E. Yamada, S. Watanabe, A.K. Hayashi, and N. Tsuboi, Proceedings of the Combustion Institute, 32, 2363–2369 (2009).
- 18) E. Yamada, N. Kitabayashi, A.K. Hayashi, and N. Tsuboi, International Journal of Hydrogen Energy, 36, 2560–2566 (2010).
- 19) Y.R. Kim, H.J. Lee, S.H. Kim, and I.S. Jeugn, Proceedings of the Combustion Institute, 34, 2057–2064 (2013).
- 20) M. Asahara, A. Yokoyama, A.K. Hayashi, E. Yamada, and N. Tsuboi, International Journal of Hydrogen Energy, 39, 20378–20387 (2014).

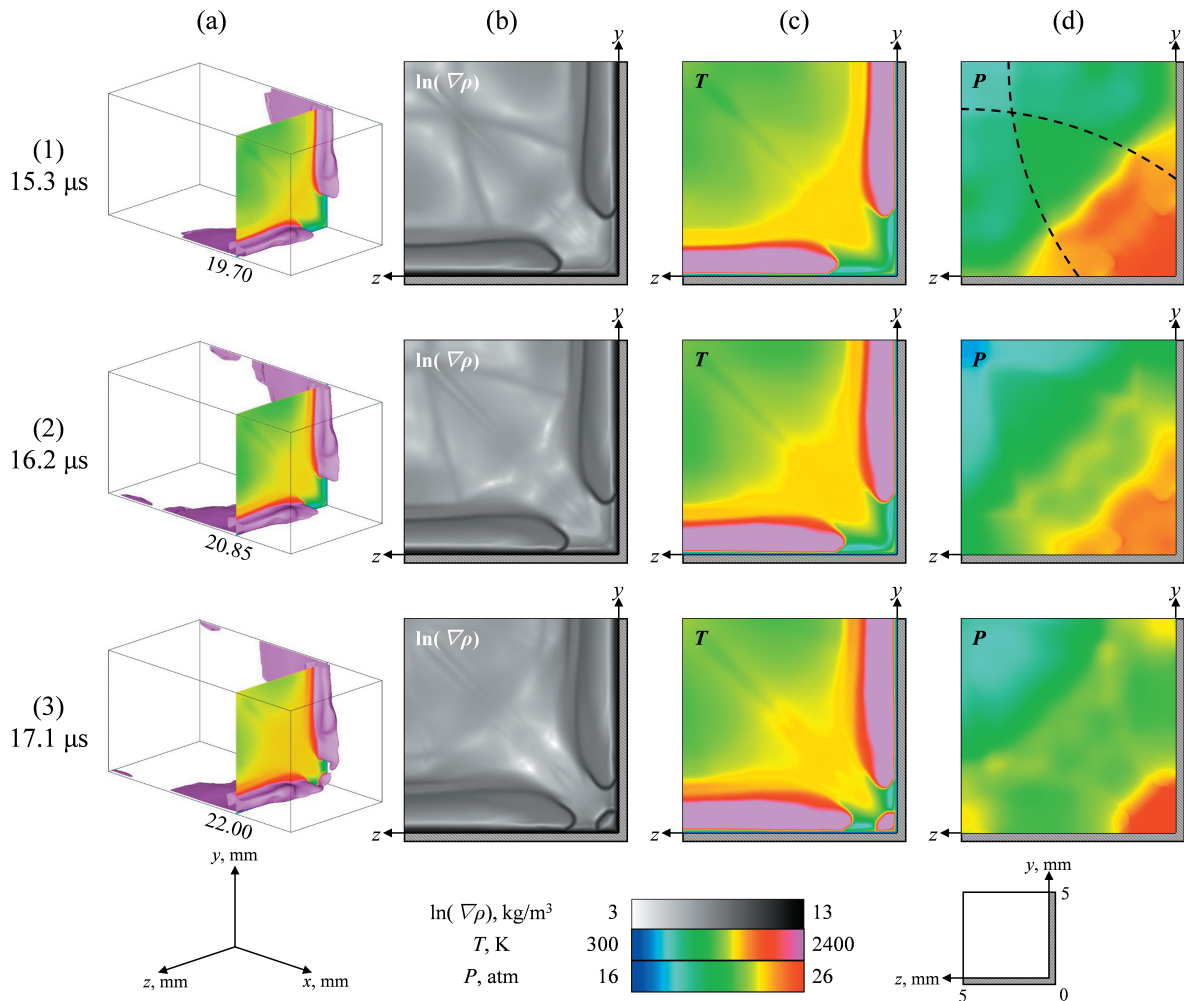


**Figure 9** Contours and isosurface, (a) : isosurface of 2400 K (b) : density gradient (c) : temperature (d) : pressure

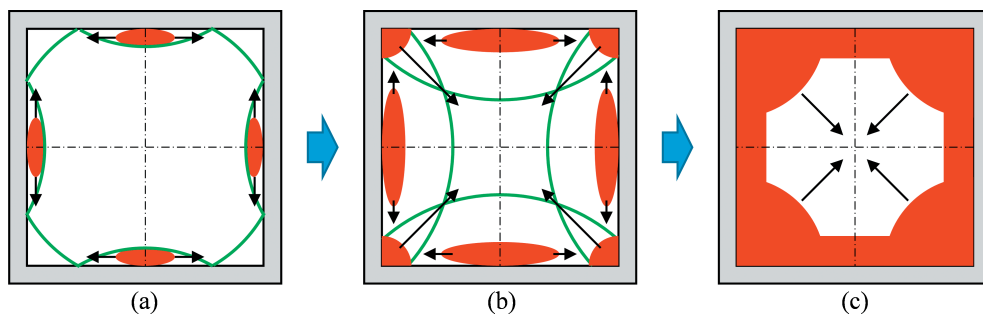


**Figure 10** Schematic figure of the transverse shock wave and the spreading flame, (a) : self-ignition at center of the wall (b) : new self-ignition at the corner of the tube (c) : spreading flame

<p>21) J. Grune, K. Sempert, M. Kuznetsov, and T. Jordan, <i>International Journal of Hydrogen Energy</i>, 39, 20396–20403 (2014).</p> <p>22) Y. Morii, H. Terashima, M. Koshi, T. Shimizu, <i>Journal of Loss Prevention in the Process Industries</i>, 34, 92–99 (2015).</p> <p>23) G. Strang, <i>Society for Industrial and Applied Mathematics Journal on Numerical Analysis</i>, 5, 506–517 (1968).</p>	<p>24) H.C. Yee, NASA Technical Memorandum, 89464 (1987).</p> <p>25) Z. Hong, D.F. Davidson, and R.K. Hanson, <i>Combustion Flame</i>, 158, 633–644 (2011).</p> <p>26) S. Chapman, T.G. Cowling, Cambridge University Press, 226–259 (1970).</p> <p>27) C.R. Wilke, A Viscosity Equation for Gas Mixtures <i>The Journal of Chemical Physics</i>, 18, 517–519 (1950).</p>
--	---